The dynamical mechanism of (111) surface reconstruction: frustration and vortex structures

1992 J. Phys.: Condens. Matter 4 8447

(http://iopscience.iop.org/0953-8984/4/44/007)

J. Phys.: Condens. Matter 4 (1992) 8447–8460. Printed in the UK

The dynamical mechanism of (111) surface reconstruction: frustration and vortex structures

Macoto Itoh

Matsushita Research Institute Tokyo, Incorporated, 3-10-1, Higashimita, Tama-ku, Kawasaki 214, Japan

Received 9 March 1992 , in final form 1 June 1992

Abstract. In terms of the antiferromagnetic XY-model on a triangular lattice in two dimensions, the mechanisms of (111) surface reconstructions of homopolar semiconductors are reconsidered. The validity of the proposed model is examined by comparing it with several experimental results, with which satisfactory agreement is obtained. In particular, the present model leads to the stability of the 5×5 and the 7×7 structures as well as a high probability of the nucleation of the $N \times N$ dimer adatom stacking-fault reconstruction from an upper step edge.

1. Introduction

By virtue of the recent development of the scanning tunnelling microscope (STM) [1], it is possible to observe the real-space configurations of surface atoms. In particular, (STM) is well suited for the observation of semiconductor surfaces, so extensive studies have been performed to investigate the surface structures of semiconductors, the most popular of which are silicon and germanium [2, 3, 4].

It is of particular interest to see that, by utilizing the above apparatus and other tools like a transmission electron microscope (TEM) [5], surface structures are shown to exhibit behaviour very different from that of the bulk. For example, silicon and germanium apparently resemble each other so closely that even the cleaved (111) surface 2×1 structures of these materials are described by the common π-bonded chain model [6–9]. Nevertheless, high-temperature annealings result in distinct reconstructed structures for each of the surfaces of Si(111) and Ge(111). They have been recognized as consisting of the 7 × 7 and the c(2 × 8) structures, respectively [5, 10–13]. Remarkably, the former structure is shown to be described by a geometrically very complicated model, the so-called dimer adatom stacking-fault (DAS) model [5], whereas the latter is confirmed by STM observations to be composed of the simple adatom registry on the bulk 1×1 [12, 13]. For the atomic arrangements of these structures, see figures 1(*a*) and 1(*b*).

It is further shown by the STM measurements that there exists a 5 × 5 DAS state on Si(111) intermediate between the 2 × 1 and the 7 × 7 DAS [14, 15].

Therefore, the purpose of the present work is to search for the driving mechanisms that lead to the structural difference between Si(111) 7×7 DAS and the Ge(111) c(2×8). In doing so, the main mechanism of the (111) surface reconstructions will be revealed.

0953-8984/92/448447+14$07.50

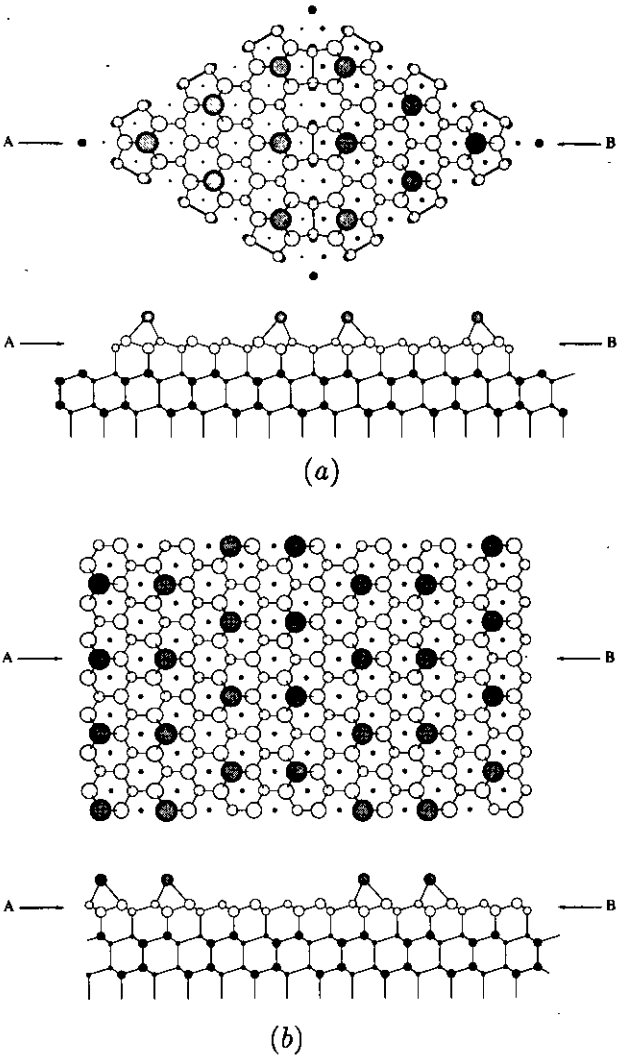

Figure 1. (*a*) The top and side views of the atomic arrangements of the Si(111) 7×7 DAS structure are depicted. The sizes of the discs decrease according to their depths. The side view shows the cross section of the top view cut along the line A–B. In both figures, adatoms are represented by the shaded discs, atoms belonging to the topmost bilayer are represented in white, and those below them are represented as dark. (*b*) The atomic arrangement of the Ge(111) c(2×8) structure is depicted. This structure is a simple adatom registry on the bulk 1×1.

Until now, there have been three known mechanisms for the (111) surface reconstructions of homopolar semiconductors. They are (*a*) surface stress, (*b*) charge transfer, and (*c*) π-bonding, among which the last works commonly on cleaved silicon and germanium surfaces to give 2×1 structures [6–8]. Since we are interested in the origin of the difference between the reconstructed Si(111) and Ge(111) structures, we hereafter discard the π-bonding effect.

The charge transfer effect between the adatom dangling bonds and the rest atom ones works well to stabilize the 2×2 structure [16, 17], whereas the relaxation of the

surface stress plays a role mostly in the presence of dimers or adatoms [17, 18]. It should be noted that neither the surface stress nor the charge transfer can drive the Si(111) surface reconstruction into the DAS structure [19]. If the stress effect can drive the DAS reconstruction, the DAS structures have to be constructed even by the extrinsic bending of a cleaved surface. While the experiments by Feenstra and Lutz indicate that the DAS reconstruction cannot be driven by the charge transfer effect [15], even in the presence of adatoms, the surface structure does not necessarily fall into the DAS reconstruction. Therefore, it seems impossible to account for the striking difference between Si(111) 7×7 DAS and Ge(111) c(2×8) on the basis of these effects alone. In particular, none of these effects can describe the formation of a single corner hole found in the upper right corner of figure 3 in [20]. At the same time, this observation also excludes the possibility of the dimer-row-driven surface reconstruction mechanism [21].

There is a widely accepted idea that reduction in the number of dangling bonds (RNDB) should be the principal mechanism governing the surface reconstructions [22]. However, this hypothesis and the above mechanisms have never been treated in a unified manner.

In the present work, we put forward this idea and adopt the assumption that the leading-order contribution to the surface reconstruction is given by following the RNDB hypothesis: the atomic arrangement of the surface is determined principally by the effect which follows directly as a consequence of this hypothesis, and the other mechanisms are assumed to work as higher-order corrections to decrease the surface free energies and to determine the correct positions of adatoms on the topmost layer. That is, we assume that the positions of the adatoms are determined by the surface stress and the charge transfer effects. Accordingly, we restrict ourselves to the structures below them, i.e. the structures in the topmost bilayer.

The reason for this is explained as follows: once the configuration of the lower half of this bilayer is determined, the upper half or the second-layer atoms of the DAS structure would be bonded onto them in a unique way by following the RNDB hypothesis. Then, under the same hypothesis, adatoms are located in the appropriate positions by the stress and the charge transfer effects. Therefore, if our assumptions are valid, the atomic configurations of the lower half of the topmost bilayer will play a key role in constructing the structures of the (111) surfaces.

In fact, these assumptions are indirectly supported by the existence of the transition temperature region far below the melting point. For instance, the melting point of Si(111) is about 1410°C, while the 7×7 reconstruction takes place in a wide region of about 500°C–860°C [14, 15, 23–25]. In this temperature region, only the surface phenomena are expected to take place. In particular, the surface atoms are expected not to migrate very much on the surface. In other words, phenomena which are important in causing the DAS reconstructions are expected to have almost nothing to do with the centre-of-mass motion of the surface atoms. If this is true, the thermal vibrations and the rotational modes would play crucial roles during the reconstructions. Of these, the thermal vibrations contribute to the removal of the atoms from the surface. Hence, if the upper half of the topmost bilayer is removed by this surface phonon mode, it becomes possible for the atoms belonging to the lower half of this bilayer to rotate on their own positions; it is this rotational mode that is discussed in the present paper.

The present paper is organized as follows. In section 2, the two-dimensional model of statistical mechanics is introduced to describe the surface dynamics. In

section 3, the results derived from the model are examined by comparing them with the experimental data. Section 4 is devoted to conclusions.

2. The model

As stated in the previous section, we concentrate on the structure of the lower half of the topmost bilayer on homopolar semiconductor (111) surfaces. In order to introduce the model, the quasi-two-dimensional approximation of the surface will also be assumed.

First, let us try to remove the topmost two layers, i.e. the adlayer and the second layer from the DAS structure in figure 1(*a*). The outermost layer of the remainder is the third layer of the DAS model; the atomic configurations of this layer are depicted in figure 2 by means of the three-pointed arrows. Since a silicon trihydride SiH_3 can rotate on Si(111) [26], it is possible to regard the three-pointed arrows in figure 2 as three-pointed planar rotators located on a two-dimensional triangular lattice.

Moreover, the interactions among them can be represented as antiferromagnetic ones. Indeed, when the wave functions of the broken covalent bonds mutually overlap with a non-zero relative angle $\Delta\theta$, the energy benefit by the bonding increases as the relative angle $\Delta\theta$ approaches π; this phenomenon can be represented with the antiferromagnetic interactions between the nearest-neighbour planar rotator pairs.

In this way, the investigation of the mechanism of (111) surface reconstructions can be recast in terms of a phase transition occurring on the three-pointed planar rotator antiferromagnetic XY-model on a two-dimensional triangular lattice. For brevity, this model will be called the 3PR–XYAFT model hereafter.

The Hamiltonian of the model is written in terms of the phase variables as

$$\mathcal{H}_{3PR} = J \sum_{(i,j)} \cos 3(\theta_i - \theta_j) + \sum_i V(\theta_i) \tag{1}$$

where J denotes the positive coupling constant, θ_i the rotation of the planar rotator on the ith site, and the summation in the first term is taken over the nearest-neighbour pairs. The first term represents the interactions among the 3PR-'classical spins', and the second term the interaction of the 'spins' with the substrate. Since the rotators are three-pointed, both terms have to be periodic with periodicity equal to $2\pi/3$, i.e. the potential $V(\theta_i)$ is invariant under the phase shift: $V(\theta_i + \frac{2}{3}\pi) = V(\theta_i)$. In accordance with figure 2, we define the 'spin' atoms in the unfaulted stacking sites as $\theta_i = (4n + 1)\pi/6$ with n a non-negative integer. Correspondingly, those atoms in the faulted stacking sites are defined as $\theta_i = (4n + 3)\pi/6$, and the constituents of the dimers are defined to be either $\theta_i = 2n\pi/3$ or $\theta_i = (2n + 1)\pi/3$. The most plausible form of the potential $V(\theta)$ in equation (1) is illustrated in figure 3.

The Hamiltonian of the one-pointed counterpart of this model is given by

$$\mathcal{H}_{1PR} = \tilde{J} \sum_{(i,j)} \cos(\theta_i - \theta_j) + \sum_i \tilde{V}(\theta_i). \tag{2}$$

By definition, this Hamiltonian is invariant under a 2π phase shift. Fortunately, this model has already been investigated by several authors, and is found to experience not only the Kosterlitz–Thouless (KT) phase transition [27,28] but also the Ising-like

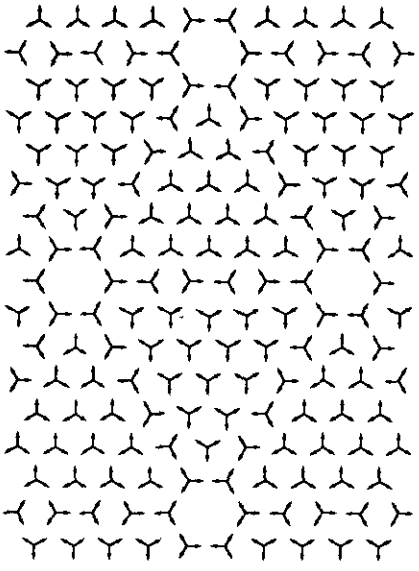

Figure 2. The ground state of the 3PR-XYAFT model is illustrated using three-pointed arrows.

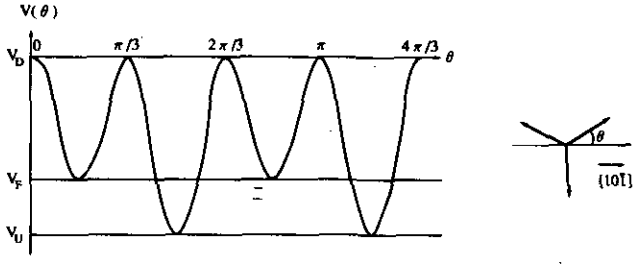

Figure 3. The potential $V(\theta)$ in equation (1) is illustrated with respect to the phase variable θ. V_U and V_F represent the potential energies corresponding to unfaulted and faulted stackings, respectively. Also, V_D is the value of the potential term $V(\theta)$ corresponding to the constituents of dimers.

second-order transition, called the chiral order [29–34]. In what follows, this model is called the one-pointed planar rotator antiferromagnetic XY (1PR-XYAFT) model.

By comparing equation (1) with equation (2), it is obvious that the difference between these Hamiltonians lies only in the difference in their periodicities. Similarly, in the corresponding order parameter spaces, it is enough to replace the symmetry group $Z_2 \otimes U(1)$ of the 1PR-XYAFT model with the group $Z_2 \otimes (U(1)/Z_3)$ of the 3PR-XYAFT model.

For later convenience, let us briefly summarize the features of the 1PR-XYAFT model in two dimensions. The Hamiltonian of the 1PR-XYAFT model is rewritten in the different form

$$\mathcal{H}_{1PR} = \tilde{J} \sum_{\langle i,j \rangle} \boldsymbol{S}_i \cdot \boldsymbol{S}_j + \sum_i \boldsymbol{H}_i \cdot \boldsymbol{S}_i \tag{3}$$

where the phase variables in equation (2) are replaced with the alternative two-dimensional vectorial ones, the components of which are the real, and the imaginary

parts of the function defined by $S_i = \exp(i\theta_i)$. In equation (3), H_i in the second term represents an external field applied to the spin configuration on the ith site.

It is well known that antiferromagnetic spin models on a triangular lattice always suffer from frustration [35–38]. That is, it is impossible for the antiferromagnetic spins on a non-bipartite lattice to take configurations in which all the spins are in antiferromagnetic states. Instead, they 'compromise' to find an alternative ground state; this is the so-called frustration. Unfortunately, such ground states are generally degenerate. In the present case, they are doubly degenerate if we neglect the trivial rotational degeneracies, so they are classified into two groups according to the sign of the chirality defined as [29–33]

$$\chi = (2/3\sqrt{3})\hat{Z} \cdot (S_1 \times S_2 + S_2 \times S_3 + S_3 \times S_1) \tag{4}$$

where the indices $i = 1, 2, 3$ of the spin variables are counted in counterclockwise order in the fundamental site and $\hat{Z}$ is a unit vector, which is the outward normal to the two-dimensional plane.

In the ground states, χ takes a value equal to either $+1$ or -1; the corresponding sites are called chiral and anti-chiral, respectively. Hence it is easily recognized that a domain boundary is expected to arise between these differently ordered domains. See figure 1 in [31].

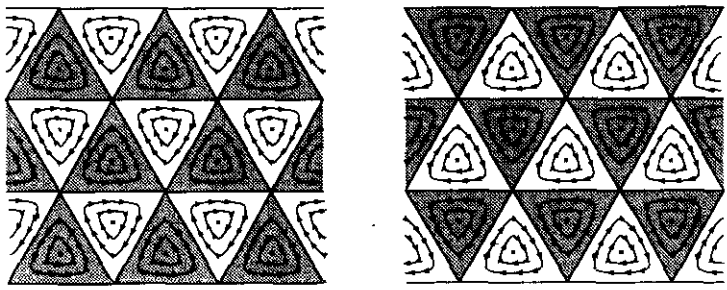

Figure 4. Two possible ground states of the ferromagnetic 1PR-XY model are illustrated. The counterclockwise winding and the clockwise winding sites are shaded and white, respectively.

In the case of the 3PR-XYAFT model, however, a vector, or a one-pointed rotator (1PR) must be replaced with a three-pointed one(3PR) [39]. Corresponding to this change, we call this Ising-like ordering the stacking ordering, which is a 3PR counterpart of the chiral ordering [39]. Likewise, the unfaulted and the faulted stacking sites of the DAS model in figure 1 correspond to the oppositely ordered domains of the chiral ordering in figure 5; these two domains are connected with the dimer rows in the DAS model.

It is obvious from the considerations above that, in analogy with the chiral ordering in the 1PR-XYAFT model, the degree of the stacking ordering in a site is specified by whether one of the three bonds of a rotator is pointing inward or outward from the site (see figure 5). In the figure, those regions pointed to by any component of the rotator are represented as dark, and others as white. Therefore, in the present model,

the unfaulted and the faulted stackings of the DAS model correspond to the ideal and the staggered configuration of the rotators with respect to the substrate.

Next, let us see the effect of the KT transition on the 3PR-XYAFT model. Below the critical temperature T_{KT} of this transition, vortices with opposite vorticities are bound together. In the usual theory of the KT transition, only the effects of the bound states with the vorticities $q = \pm 1$ are taken into account. This is because it is energetically less favourable to excite the configuration with the higher-order vorticities [27,28].

However, as the temperature decreases from criticality, the nature of the underlying lattice will no longer be ignorable. That is, since the 3PR-XYAFT model is defined on a triangular lattice, only the vortices that are compatible with the symmetry of the lattice are allowed to survive at low temperatures. By taking into account the existence of two distinct stackings in the 3PR-XYAFT model, it is concluded that the $q = -2$ and the $q = +1$ vortices are the only allowed topological configurations in the boundary-free regions on the lattice [40] (see figure 6). For clarity, the figures are illustrated in terms of the streamlines of the ferromagnetic XY-model. As is easily seen from the third row of the figures, the $q = -1$ configuration is not allowed to take place in this region.

Thus, the most stable vortex configuration at sufficiently low temperatures has to be identical to the structure shown in figure 2, the corresponding configurations of which for the ferromagnetic 1PR model are those shown in figure 4. Comparison of figure 2 with figure 4 shows that the singularities are present at the centres of the unfaulted and the faulted triangular sites of the configuration in figure 2 as well as at the centres of the corner holes; presumably this is why the third-layer atoms are absent from the corners of the DAS structure in figure 1(*a*).

From these considerations, it is clear that the threefold symmetry of the reconstructed Si(111) $N \times N$ DAS structure comes both from the symmetries of the substrate and the planar rotators placed on it.

In contrast to the above, the $q = -1$ vortices are also allowed to exist on a lattice with a boundary. Illustrated at the bottom of figure 6 are the two possible $q = -1$ configurations at the boundary regions of the upper half plane. The boundary effect will be considered again in the next section.

3. Examining the model

It is important to examine whether the proposed model is realistic in describing the

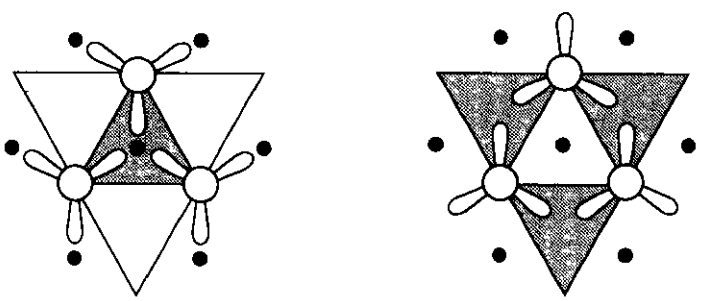

Figure 5. Two possible ground states of the 3PR-XYAFT model are depicted. The atoms belonging to the next bilayer are represented by the black dots. Those sites into which the rotators are pointing are represented by the shaded triangles, whereas the empty ones are represented by the white triangles.

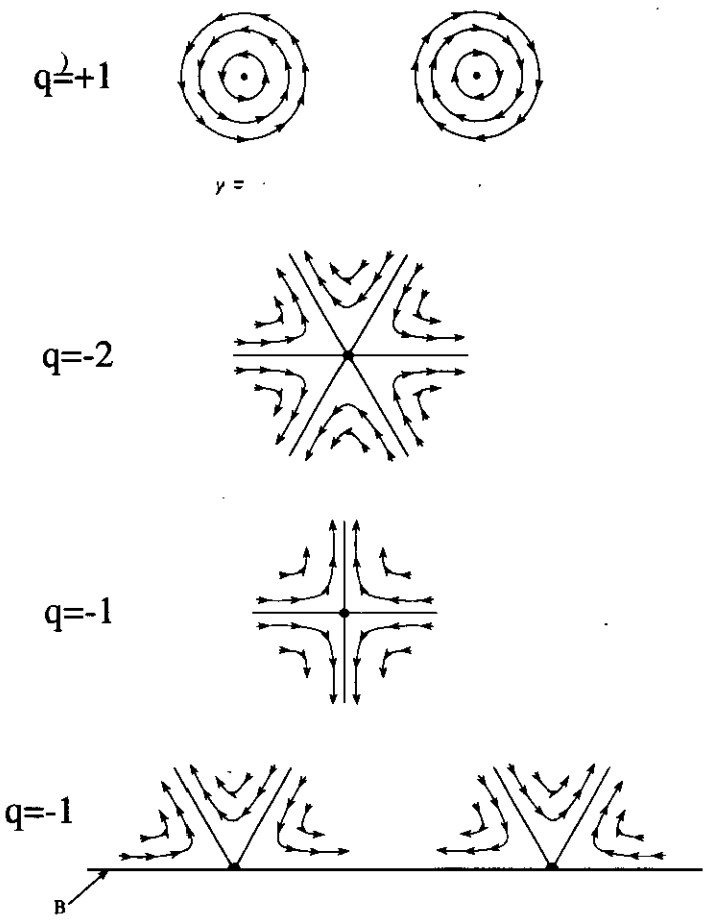

Figure 6. In terms of the streamlines of the ordinary ferromagnetic 1PR-XY model, $q = +1$, $q = -2$ and $q = -1$ vortices are illustrated in the first, second, and third rows, respectively. Only configurations of the former two kinds are compatible with the triangular lattice, while $q = -1$ vortices are allowed on the same lattice only in the boundary region. In the fourth row B denotes the boundary edge, and two kinds of $q = -1$ vortices are illustrated at the boundary edge of an upper half-plane.

typical properties of the (111) surface reconstructions. In what follows, comparison is made between the results derived from the 3PR-XYAFT model in equation (1) and representative experimental data.

First, as shown in [31,32] for the 1PR-XYAFT model, the allowed 'spin' configuration of the 3PR-XYAFT model has to be either an $N \times N$ DAS structure or a simple 1×1 that is identical to the bulk structure; the resulting structure depends on the strength of 'spin–spin' interaction relative to the coupling of the 'spins' to the substrate in equation (1). More precisely, let us denote the energy difference between the unfaulted and the faulted stackings as ΔV, i.e. $\Delta V = |V_F - V_U|$ (see figure 3), and its ratio to the 'spin–spin' coupling constant J as κ; $\kappa = \Delta V/J$. Then, if the value of this parameter κ exceeds the critical value κ_C, the transition necessarily results in the formation of the 1×1, identical to the unreconstructed ideal structure.

In contrast, if the value of κ is less than κ_C, the configuration reconstructs into the $N\times N$ DAS structure with a certain value of N. Besides, according to the RNDB hypothesis, Ns have to be odd integers. Otherwise many broken bonds would be left on the surface; obviously, this contradicts the hypothesis.

Second, the lower bound on the size of a unit cell of $N\times N$ DAS can be easily derived from the model. Since the singular points are located on the lattice at the

positions of the centres of $q = +1$ and $q = -2$ vortices, the value of N is restricted to being larger than or equal to 5 [14,15,41]. Otherwise, two different singularities $q = +1$ and $q = -2$ would overlap, and this would result in the formation of a $q = -1$ vortex, which is incompatible with a triangular lattice in the boundary-free region. Thus, as long as our approximation of the quasi-two-dimensionality of the surface holds, the inequality $N \geqslant 5$ is guaranteed.

Generally, the $N \times N$ DAS structures with $N = 6k + 3$ ($k = 0, 1, 2, \ldots$) cannot be stable as widely spread two-dimensional configurations; in these configurations, the 'spin' atoms, i.e. the third-layer atoms of the DAS structure, have to be present at the centres of the triangular sites. However, this is evidently not allowed, because the $q = +1$ singularities are present at just the same positions.

Concerning this, it is interesting to see that the first term of the Hamiltonian in equation (2) can be rewritten in the classical Coulomb gas picture into the following form [27,28,42]:

$$\mathcal{H}_{1PR} \sim -\pi \bar{J} \sum_{i \neq j} q_i q_j \log | z_i - z_j | + \text{irrel.} \tag{5}$$

where z_i denotes the position of the centre of the ith vortex expressed as a complex number, and q_i denotes the vorticity or 'the electric charge' of the ith vortex. In equation (5), irrelevant terms in our discussion are neglected.

Since the accuracy of this expression is guaranteed, at least near criticality, it can be concluded from this expression that the positively and the negatively charged vortices attract each other. In other words, once the DAS structure is formed, those with smaller unit cells are energetically favoured over those with larger unit cells. Besides, the formation of the $N \times N$ DAS with $N = 6k + 3$ are shown to be unfavourable. Thus, if a large area of a (111) surface is covered with an $N \times N$ DAS structure, the value of N must be either 5 or 7, for which the 5×5 DAS structure has intrinsic advantages. Therefore, when the higher-order contributions such as the stress effects can be neglected, or if the two-dimensional character of the system becomes dominant, the 5×5 DAS structure will be realized more easily than the 7×7 DAS structure.

Note that this result does not exclude the occurrence of the $N \times N$ DAS structures with $N > 7$. Actually, small domains of 9×9 DAS structures have been observed on Si(111) [43,25]. This is possible because, after the incorporation of the adatoms, the system is no longer two-dimensional, so the vorticities (which are the two-dimensional invariants) cannot be preserved. In contrast, the formation of the 3×3 DAS structure is strongly forbidden, because this structure is unfavourable even in the *ab initio* energy calculations including all the elements of the DAS structure [41–43]. Indeed, in the experiments, only one unit cell of the 3×3 DAS structure was reported in figure 7 of [47].

Third, many experiments using molecular beam epitaxy (MBE) have revealed that hetero-epitaxially grown surfaces and ordinary or homo-epitaxially grown surfaces often exhibit different structures. For instance, Ge(111) and Si(111) surfaces reconstruct into Ge(111) c(2×8) and Si(111) 7×7 DAS structures respectively, and the homo-epitaxially grown Si/Si(111) surface exhibits again the 7×7 DAS structure, whereas the hetero-epitaxially grown Ge/Si(111) surface exhibits the 5×5 DAS structure [41]. This phenomenon is conventionally explained as having been induced by the surface strain effect.

However, in the present approach, what is responsible for this structural change is not the strain but the difference in melting point. Since the melting point of germanium is much lower than that of silicon, an almost ideal two-dimensional system is realized for the hetero-epitaxially grown Ge/Si(111) surface. More precisely, the difference in melting point between the two distinct elements creates a temperature region in which an almost pure manifestation of the surface phenomenon is achieved. In this case, the reconstruction is expected to fall into the formation of the 5×5 DAS structure. Evidently, the same reasoning also applies to the low-temperature annealing of the cleaved Si(111) surface, which is shown to lead to the formation of the 5×5 DAS structure too [14,15].

Fourth, it is easy to account for the formation of a single corner hole on Ge(111) in the upper right-hand corner of figure 3 in [20], as well as those found on the low-temperature-annealed Si(111) cleaved surface [14,15], and those on the homo-epitaxially grown silicon islands on the Si(111) surface [47].

Since the ordinary structure of a Ge(111) surface is stacking-fault free, the second term in equation (1) seems to govern the Ge(111) surface, i.e. the inequality $\kappa > \kappa_C$ would hold. However, there remains the possibility that a fluctuation creates a single vortex among the well-ordered domains of 1×1 structures. Then, during the cooling, the bonding of the other atoms onto the rotators would fix and freeze the 'spin' configuration, and the isolated corner holes would be enabled to survive even at room temperature.

Fifth, as stated in section 2, attention must also be paid to the boundary effects. Of the many possibilities, the simplest case is that of the surface phenomenon near an upper step edge. In two-dimensional statistical mechanics, the effect of an upper step edge can be taken into account by considering the boundary effect. So it is enough to consider, for instance, the model on the two-dimensional upper half plane.

As mentioned in the previous section, the $q = -1$ vortices are allowed to exist on a triangular lattice only at the boundary edge. Furthermore, there are two kinds of configuration for them. See figure 6 again. As is the case for the $q = +1$ vortices, the configurations with a larger number of unfaulted stacking sites than faulted ones are energetically favoured over those for which the opposite holds. This is due to the existence of the second term in equation (1).

Since the $q = -1$ vortices are energetically favoured over the $q = -2$ ones, it is much easier to form a vortex lattice here than to do so at any other place on the surface. Therefore, the nucleation of the DAS structure is expected to start at an upper step edge with substantially higher probability than in the central region of a terrace [24,48].

Sixth, low energy electron reflection microscope (LEERM) observation showed that the reconstructed regions of the 7 × 7 DAS structures develop in the disordered sea of '1 × 1' states in the shape of equilateral triangles, with the apices pointing in the $[11\bar{2}]$ direction [24,49,50].

This fact indicates that, of two possible triangles, those with the $[11\bar{2}]$ direction are definitely selected. In other words, the definite alignment of the regular triangles means the occurrence of the symmetry breaking, i.e. during the reconstruction, a second-order phase transition is also taking place. In the framework of the model described in section 2, the occurrence of this phenomenon is easily explained, because not only the KT transition but also the Ising-like phase transition (i.e. that relating to the stacking order) takes place in the 3PR-XYAFT model. Further support for this interpretation can be obtained from the low energy electron diffraction (LEED)

experiment performed by Bennet and Webb [51]. They estimated the critical exponent β of the '1 × 1' to 7×7 transition to be $\beta = 0.11 \pm 0.015$ [51], which is very close to the value 0.125 for the Ising model in two dimensions. Moreover, they found two critical temperatures. Besides the critical temperature $T_C = 1140\,\mathrm{K}$ above which the true disordered state seems to be realized, they found the critical temperature of the Ising-like phase transition to be $T_C' = 1126 \pm 2\,\mathrm{K}$.

According to the present model, these two critical temperatures are interpreted as those of the KT transition and the stacking order. Correspondingly, the following three phases seem to be realized: (i) when $T > T_C$, vortices are unbound and single vortices are moving on the surface; (ii) when $T_C' < T < T_C$, the $q = \pm 1$ vortices are predominantly bound together; (iii) when $T < T_C'$, the $q = -2$ vortices are realized as the bound states of the $q = -1$ ones, and the $q = +1$ and the $q = -2$ vortices are bound together to form a vortex lattice, and hence the DAS structure is formed [27,28]. The realization of the second phase is possible because the detailed character of the underlying lattice is irrelevant for the dynamics near criticality.

In relation to these phenomena, it is interesting to see the theoretical results derived for the 1PR-XYAFT model by Miyashita and Shiba [30]; they estimated the critical temperatures of the 1PR-XYAFT model as $T_{KT} \simeq 0.502 J_{1PR}$ and $T_\chi \simeq 0.513 J_{1PR}$ [30]. Here, T_{KT} and T_χ denote the critical temperatures of the KT transition and the chiral ordering of the 1PR-XYAFT model, respectively. While these are not in agreement with those estimated by Bennet and Webb [51], the calculated results of Lee *et al* [32] are in good agreement with them.

To be precise, the results of Lee *et al* are

$$T_{KT} = (0.510 \pm 0.005) J_{1PR} \qquad T_\chi = (0.505 \pm 0.005) J_{1PR}$$

and the ratio is $T_{KT}/T_\chi = 1.01 \pm 0.02$.

On the other hand, the ratio of the experimentally estimated temperatures obtained by Bennet and Webb is $1140/1126 = 1.01$. They are thus in good agreement with each other.

Based on the fact that the nucleation of the 7×7 domain initiates from an upper step edge, Osakabe *et al* insisted that the phase transition between the 1×1 and the 7×7 phases is a first-order transition [48]. However, the order of the transition does not depend on the place where a transition begins. Moreover, Telieps and Bauer reported the results of the observation by LEERM, in which the transitions are seen to start not only from upper step edges but also in the central region of the terrace [50]. Based upon this observation, Telieps and Bauer [50] also insisted that the phase transition must be of first order. Their conclusion rests on the apparent phase separation between the 1 × 1 and the 7 × 7 phases. However, the lateral resolution of the LEERM is 20 nm at best [52], so the precursor ordering phenomenon is indistinguishable using this apparatus, because the length scale of the 7×7 DAS structure is only about 3 nm.

Instead, it seems that the expected precursor ordering has already been observed in figure 7 of [15], in which several single corner holes are seen to be distributed in the disordered areas of adatoms.

If the possibility of a weak first-order transition is to remain for the whole transition of the DAS reconstruction, the energy corresponding to the latent heat has to be supplied by the kinetic energies of the atoms other than the planar rotators. However, since the kinetic energies of these atoms are expected to be tiny, it is rather

implausible to consider the transition to be first-order, though the possibility of the first-order transition is not completely excluded.

Finally, according to the present model, the well-known 1×1 LEED pattern in the high-temperature phase is attributed to the existence of the rotators, since they rotate in their own 1×1 positions.

4. Conclusion

In order to study the (111) surface reconstructions, the two-dimensional statistical mechanical model, i.e. the 3PR-XYAFT model, is introduced. In building the model, the surface atoms having three broken covalent bonds are represented by the three-pointed planar rotators. At first glance, this simplification seems too drastic. However, since any covalent bonds connecting two neighbouring atoms are likely to be as straight as possible, this assumption seems physically meaningful.

On the basis of the present model, the following results are derived:

(i) After enough annealing, the reconstruction of the homopolar semiconductor (111) surfaces necessarily leads to the formation of either the 1×1 or the $N \times N$ DAS structure with an odd-integer value of N.

(ii) The value of N must be larger than or equal to 5. In particular, the value of this integer is restricted to the range $5 \leqslant N \leqslant 7$ for the stable structures.

(iii) The nucleation of the DAS reconstruction can easily begin at an upper step edge.

(iv) The corner holes of the DAS structures are the topological excitations.

(v) Hetero-epitaxially grown Ge 5×5 DAS/Si(111) is enabled to be formed due to the difference in melting point of germanium and silicon.

(vi) The critical exponent $\beta = 0.11 \pm 0.015$ and the critical temperature $T_C' = 1126 \pm 2\,\mathrm{K}$ reported by Bennet and Webb [51] would be the result of the Ising-like second-order phase transition contained in the model, whereas the transition at $T_C = 1140\,\mathrm{K}$ would correspond to the KT transition.

(vii) The 1×1 LEED pattern in the high-temperature phase is attributed to the existence of the planar rotators.

All of these results are in good agreement with the known experiments. The first one excludes the possibilities of both the dimer chain model [53, 54] and the parallel dimer wall model [55].

In the LEERM observations, two different shapes of the reconstructing regions are found; the compactly growing equilateral triangles are reported in [24, 49, 56], whereas in [50] threefold symmetric dendritic growth is reported. In both cases, the apices of the polygons are pointing in the [11$\bar{2}$] direction. According to the present model, this difference in the growth shapes may be accounted for as the result of the Coulomb force in equation (5) and the crossover of the Ising-like character which interpolates between the dendritic growth in the nucleation of an ordered domain and the compact growth appearing in the latter regime [57].

Thus, the 3PR-XYAFT model is a convincing model which can describe the driving mechanism of homopolar semiconductor (111) surface reconstructions.

Note that these results are derived under the following assumptions.

(i) Reduction in the number of dangling bonds is the principal mechanism of surface reconstructions.

(ii) Well-known surface effects such as the surface stress or the charge transfer are higher-order corrections minimizing the surface energy.

(iii) Below the melting temperature, there is a sufficiently wide temperature range in which only the thermal vibrations and the rotations of surface atoms are expected to play significant roles.

The last assumption ensures that the surface atoms are in a state of thermal fluctuation about their own positions in some temperature range, above which the surface atoms are expected to leave their positions so that the whole system falls into a melting state.

By making use of the 3PR–XYAFT model, it can be made clear that the Si(111) surface reconstruction results in the formation of the DAS structure because the frustration effect works on this surface and the vortices play the role of the precursors of the phase transition.

The conventional explanation of (111) surface reconstructions seems to be incorrect, i.e. one cannot explain in terms of the strain effect alone, why the reconstructed structures again have a three-fold symmetry. Rather, it was shown theoretically that dimers are always accompanied by adatoms because the stress effects caused by the formation of dimers and the location of adatoms are both tensile [17, 18]. This suggests the combined use of the 3PR–XYAFT model and the surface stress as well as the charge transfer. It would be natural to think that the vortices play the role of the precursor, but the construction and the stabilization of the whole of the DAS structure are assisted by the surface stress and the charge transfer effects. Perhaps this is the true reason why the size of a unit cell of a DAS structure depends on the presence of extra adatoms [15].

Finally, comparison of the results derived from the present model with the experiments by Feenstra and Lutz in [15] reveals the possibility that the successive STM observations of atomic behaviour on a silicon-deposited cleaved surface during low-temperature annealing will reveal how the KT transition proceeds in real-space experiments. This is because the atomic configuration can be fixed whenever the annealing is stopped, and thus the transition process itself can be stopped. Alternatively, the precursor ordering and the KT transition will be observed in the disordered phase by high-temperature STM observation [58].

Acknowledgments

The author would like to thank Professor M Suzuki for fruitful discussion and reading the manuscript, Professor T Saso for discussion and Professor S Takagi for correspondence. He would also like to thank Dr R Sano, M Nakajima and I Sumita for their encouragement.

References

[1] Binning G, Rohrer H, Gerber Ch and Weibel E 1982 *Phys. Rev. Lett.* **49** 57
[2] Becker R S, Golovchenko J A, Hamann D R and Swartzentruber B S 1985 *Phys. Rev. Lett.* **55** 2032
[3] Hamers R J, Tromp R M and Demuth J E 1986 *Phys. Rev. Lett.* **56** 1972
[4] Becker R S, Golovchenko J A and Swartzentruber B S 1985 *Phys. Rev. Lett.* **54** 2678
[5] Takayanagi K, Tanishiro Y, Takahashi S and Takahashi M 1985 *Surf. Sci.* **164** 367; 1985 *J. Vac. Sci. Technol.* A **3** 1502
[6] Pandey K C 1981 *Phys. Rev. Lett.* **47** 1913; 1982 *Phys. Rev. Lett.* **49** 223

[7] Vanderbilt D and Louie S G 1985 *The Structure of Surfaces (Springer Series in Surface Sciences* **2***)* ed M A van Hove and S Y Tong (Berlin: Springer) p 29
[8] Northrup J E and Cohen M L 1983 *Phys. Rev.* B **27** 6553
[9] Feenstra R M, Thompson W A and Fain A P 1986 *Phys. Rev. Lett.* **56** 608; 1986 *J. Vac. Sci. Technol.* A **4** 1315
[10] Schlier R E and Farnsworth H E 1959 *J. Chem. Phys.* **30** 917
[11] Palmberg P W and Peria W T 1967 *Surf. Sci.* **6** 57
[12] Becker R S, Swartzentruber B S, Vickers J S and Klitsner T 1989 *Phys. Rev.* B **39** 1633
[13] Feenstra R M and Lutz M A 1991 *Surf. Sci.* **251/252** 401
[14] Feenstra R M and Lutz M A 1990 *Phys. Rev.* B **42** 5391; 1991 *J. Vac. Sci. Technol.* B **9** 716
[15] Feenstra R M and Lutz M A 1991 *Surf. Sci.* **243** 151
[16] Northrup J E 1986 *Phys. Rev. Lett.* **57** 154
[17] Meade R D and Vanderbilt D 1989 *Phys. Rev. Lett.* **63** 1404
[18] Payne M C 1987 *J. Phys. C: Solid State Phys.* **20** L983
[19] Vanderbilt D 1987 *Phys. Rev. Lett.* **59** 1456
[20] Feenstra R M, Slavin A J, Held G A and Lutz M A 1991 *Phys. Rev. Lett.* **66** 3257
[21] Vanderbilt D 1987 *Phys. Rev.* B **36** 6209
[22] See for example, Pandey K C 1983 *Physica* B **117/118** 761
[23] See for example, Haneman D 1987 *Rep. Prog. Phys.* **50** 1045
[24] Telieps W and Bauer E 1986 *Ber. Bunsenges. Phys. Chem.* **90** 197
[25] Feenstra R M and Lutz M A 1991 *The Structure of Surfaces III (Springer Series in Surface Sciences* **24***)* ed S Y Tong and M A van Hove (Berlin: Springer) p 480
[26] Pandey K C, Sakurai T and Hagstrum H D 1975 *Phys. Rev. Lett.* **35** 1728
[27] Kosterlitz J M and Thouless D J 1973 *J. Phys. C: Solid State Phys.* **6** 1181
[28] Kosterlitz J M 1974 *J. Phys. C: Solid State Phys.* **7** 1046
[29] Miyashita S 1986 *J. Phys. Soc. Japan* **55** 3605
[30] Miyashita S and Shiba H 1984 *J. Phys. Soc. Japan* **53** 1145
[31] Lee D H *et al* 1984 *Phys. Rev. Lett.* **52** 433
[32] Lee D H *et al* 1986 *Phys. Rev.* B **33** 450
[33] Kawashima N and Suzuki M 1989 *J. Phys. Soc. Japan* **58** 3123
[34] Kawamura H 1986 *J. Phys. Soc. Japan* **55** 2095
[35] Toulouse G 1977 *Commun. Phys.* **2** 115
[36] Villain J 1977 *J. Phys. C: Solid State Phys.* **10** 1717;4793
[37] Teitel S and Jayaprakash C 1983 *Phys. Rev.* B **27** 598
[38] Forgacs G 1980 *Phys. Rev.* B **22** 4473
[39] Itoh M 1992 unpublished
[40] See for example, Mermin D 1979 *Rev. Mod. Phys.* **51** 591
[41] Ichikawa T and Ino S 1984 *Surf. Sci.* **136** 267
[42] See for example, Itzykson C and Zuber J B 1989 *Statistical Field Theory* (Cambridge: Cambridge Univ Press) ch 4
[43] Becker R S, Golovchenko J A, Higashi G S and Swartzentruber B S 1986 *Phys. Rev. Lett.* **57** 1020
[44] I. Štich *et al* 1992 *Phys. Rev. Lett.* **68** 1351
[45] Brommer K D *et al* 1992 *Phys. Rev. Lett.* **68** 1355
[46] Adams G B and Sankey O F 1991 *Phys. Rev. Lett.* **67** 867
[47] U. Köhler, Demuth J E and Hamers R J 1989 *J. Vac. Sci. Technol.* A **7** 2860
[48] Osakabe N, Tanishiro Y, Yagi K and Honjo G 1981 *Surf. Sci.* **109** 353
[49] Bauer E, Mundschau M, Swiech W and Telieps W 1991 *J. Vac. Sci. Technol.* A **9** 1007
[50] Telieps W and Bauer E 1985 *Surf. Sci.* **162** 163
[51] Bennet P A and Webb M B 1981 *Surf. Sci.* **104** 74
[52] Telieps W and Bauer E 1985 *Ultramicroscopy* **17** 57
[53] Takayanagi K, Tanishiro Y and Kajiyama K 1986 *J. Vac. Sci. Technol.* B **4** 1074
[54] Takayanagi K and Tanishiro Y 1986 *Phys. Rev.* B **34** 1034
[55] Hao Y G and Roth L M 1990 *Surf. Sci. Lett.* **232** L201
[56] Mundschau M, Bauer E, Telieps W and Swiech W 1990 *Phil. Mag.* A **61** 257
[57] Sørensen E S, Fogedby H C and Mouritsen O G 1988 *Phys. Rev. Lett.* **61** 2770
[58] Kitamura S, Sato T and Iwatsuki M 1991 *Nature* **351** 215